1. Narongchai Thodsaporn[1], 2. Vijit Kinnares[1], 3. Papol Sardyoung[2]

Department of Electrical Engineering, School of Engineering, King Mongkut's Institute of Technology Ladkrabang (1)
Faculty of Industrial Technology, Thepsatri Rajabhat University (2) Thailand
ORCID.

doi:10.15199/48.2021.11.14

Grid Connected Unsymmetrical Two-Phase Induction Generator System Using Time-Based Unbalanced Space Vector PWM and Adaptive Hysteresis Band Current Control

Abstract. *This paper presents performance analysis of a single-phase grid conneted unsymmetrical two-phase induction generator. A voltage doubler bidirectional AC-DC converter for a grid side allowing regenerative operation is controlled by an adaptiptive band hysteresis current controller in order to improve power quality particulrly a reduction in current ripple. For a machine side, a two-phase three leg voltage source converter with time-based space vector PWM offers unbalanced orthogonal two-phase voltages for variable frequency excitation to enhance performance of the generator compared with balanced ones. Comparative performance analysis between time-based space vector PWM schemes for both balanced and unbalanced two-phase voltages using both simulation and experiment is demonstrated under various operating conditions. The simlation and experimental results are in good agreement. It is found that the unbalanced space vector PWM outperforms balanced one over a wide range of operation.*

Streszczenie. *W artykule przedstawiono analizę pracy jednofazowego, niesymetrycznego, dwufazowego generatora indukcyjnego połączonego z siecią. Dwukierunkowy konwerter AC-DC podwajający napięcie po stronie sieci, umożliwiający pracę regeneracyjną, jest sterowany przez adaptacyjny regulator prądu histerezy pasma w celu poprawy jakości energii, a zwłaszcza zmniejszenia tętnienia prądu. Po stronie maszyny dwufazowa trójnożna przetwornica źródła napięcia z czasowym wektorem przestrzennym PWM oferuje niesymetryczne ortogonalne napięcia dwufazowe do wzbudzania o zmiennej częstotliwości w celu zwiększenia wydajności generatora w porównaniu ze zrównoważonymi. Zademonstrowano porównawczą analizę wydajności między schematami PWM opartych na wektorze przestrzennym w oparciu o czas dla zarówno zrównoważonych, jak i niezrównoważonych napięć dwufazowych, z wykorzystaniem zarówno symulacji, jak i eksperymentu, w różnych warunkach pracy. Wyniki symulacji i eksperymentów są zgodne. Stwierdzono, że niezrównoważony wektor przestrzenny PWM przewyższa zrównoważony w szerokim zakresie działania.*
(Podłączony do sieci niesymetryczny, dwufazowy system generatora indukcyjnego wykorzystujący niesymetryczny przestrzenny wektor PWM oparty na czasie i kontroli prądu w paśmie histerezy adaptacyjnej)

Keywords: Unsymmetrical two-phase induction generator, space vector PWM, three-leg voltage source inverter.
Słowa kluczowe: Niesymetryczny dwufazowy generator indukcyjny, wektor przestrzenny PWM, trójnożny falownik źródła napięcia.

Introduction

A single-phase induction motor (SPIM) is commonly used in low power household appliances such as pumps, refrigerators, hand tools, blowers and so on [1]. In those applications, the SPIM operates at fixed frequency supplied from the ac grid resulting in single speed operation. As a consequence energy saving, low torque pulsations, variable speed and high efficiency cannot be achieved. In order to improve the performance of an existing SPIM, it can be adapted to an unsymmetrical two-phase induction motor (UTPIM) by disconnecting from each other of terminals of main and auxiliary windings and removing capacitors from an auxiliary winding of a capacitor run SPIM [2, 3, 4, 5, 6]. Then both windings can be supplied by various topologies such as two-leg, three-leg, or four-leg voltage source inverters (VSIs) providing orthogonal two-phase voltages for variable frequency drives. Subsequently energy saving, reduced torque pulsations and higher power rating can be achieved [7]. A squirrel cage induction generator is likely to be used in large scale applications in electricity generation from renewable energy sources like wind and hydro which are clean and less pollution [8, 9, 10,11]. In order to improve performance of a generator to meet requirements of effective energy conversion such as maximum power point tracking and a wide range of turbine speeds (i.e. from cut-in to cut-out speeds), improved power factor, power electronic converters are needed [1, 2]. Several attempts have been made to bring a three-phase induction machine to operate as not only a single-phase self excited induction generator for variable speed drive applications but also a single-phase induction generator for grid connection using an AC-DC-AC converter system instead of direct connection where a three-phase system is not available [13, 14]. A small scale generator is generally used as a single-phase mains supply for stand alone applications in rural areas. However, the counterparts for this application especially wind energy conversion are permanent magnet synchronous generators like axial flux permanent magnet synchronous generator offering some advantages especially in efficiency over the single-phae induction generator (SPIG) [15]. A small scale single-phase induction generator with direct grid connection encounters a problem of poor grid power factor particularly at low power transfer. As a consequence, capacitors for power factor correction is required. Due to imperfect of such devices, harmonic currents are present [15, 16]. Furthermore, it requires a soft starter to reduce inrush current during start up. Thus an AC-DC-AC converter system is essential to improve such performance. Moreover, control of maximum power tracking of wind energy conversion can be accomplised with this topology. Current controlled VSI is widely used in active filters, motor drives, renewable energy conversion systems since it offers simplicity of implementation, fast response, and inherent-peak current limiting capability [17, 18, 19, 20]. Various hysteresis band current control techniques can be found in [3, 18, 21]. Fixed hysteresis band current control for single-phase grid connection with multifunctionality of active and reactive power transfer and harmonic compensation for photovoltaic and wind energy conversion can also be found in [17, 22]. However, due to lack of constant DC voltage control, these systems could encounter a stability problem. A space vector pulse width modulation (SVPWM) technique is well established for three-phase inverter fed induction motor. SVPWM based two-leg, three-leg and four-leg VSIs for variable speed drives of an unsymmetrical two-phase induction motor were reported in [6, 23, 24]. Also, independent speed control of two SPIMs employs a five-leg inverter in order to reduce

number of switches and cost [9]. An unbalanced SVPWM technique for two-phase three-leg VSI for driving a TPIM has proved the better performance over balanced SVPWM in terms of lower torque pulsations and higher average electromagnetic torque [6, 24]. However, there are a few publications focusing on unsymmetrical two-phase induction generator (TPIG). The enhanced drive system for exciting stator windings of an unsymmetrical TPIG with unbalanced voltages has not been reported yet. Although the performance of unsymmetrical two-phase induction machines operates in motoring and generating modes was reported in [2], the effect of SVPWM strategies on ripple of dc link voltage controlled by a voltage doubler bidirectional rectifier with improved power qualty of the grid has not been investigated. Therefore, this paper aims at improving performance of an unsymmetrical induction generator with the merits of adaptive hysteresis band current control and unbalanced SVPWM scheme. This paper is organized as follows. Firstly, system description is given. Secondly, characteristics of a two-phase generator are explained. Then adaptive hysteresis band current control modified from a conventional fixed band technique is described. After that, the implementation of unbalanced SVPWM is given. Then simulation and experimental results of comparison between both SPWM schemes under various operating conditions are discussed. Also, the improved grid current waveforms are demonstrated. Finally, conclusion is included.

System description

As shown in Fig.1, the proposed system for grid connection mainly consists of a machine side converter (MSC) using a two-phase three-leg inverter based on SVPWM, a grid side converter (GSC) using double voltage configuration based on adaptive hysteresis current control, a two-phase induction generator (TPIG), a DC motor controlled with a DC drive with torque control acting as a prime mover. The DC link voltage is kept constant using adaptive hysteresis band current control resulting in near unity power factor and nearly sinusoidal current waveform of the grid. For control of excitation of the generator, both balanced and unbalanced SVPWM schemes are generated with variable voltage and variable frequency (VVVF) for the MSC. The control algorithms are implemented on two TMS320C2000 F28335 microcontroller boards for flexibility and independent control of both side converters.

Unsymmetrical Two-Phase induction generator

As mentioned earlier, the unsymmetrical TPIG was modified from an existing single-phase capacitor run induction motor by removing a capacitor from an auxiliary winding which main and auxiliary stator windings are displaced in space by 90 electrical degrees. Generally, both windings have different impedances due to the purpose of self starting of SPIM when is supplied by a single-phase ac source. Equivalent circuit for both windings of a TPIG modified from that of an TPIM for determining performance is shown in Fig.2 [3]. The slip s is negative since the rotor speed is higher than the synchronous speed related to the excitation frequency. The corresponding phasor diagram is also illustrated in Fig.3. Auxiliary and main winding voltages are orthogonal supplied by a two-phase voltage source.

For unbalanced case, the magnitude of the auxiliary voltage is equal to turns ratio times that of the main winding. Subsequently, magnetomotive force (mmf) for each phase is equal (i.e. treated as a symmetrical two-phase machine). The backward component of the air-gap flux is absent, thus decreasing the motor iron losses [7]. Moreover, low torque pulsations and higher output power for the same motor rating can be obtained. The current equation for both windings of an unsymmetrical TPIG is

$$I_m = aI_a \tag{1}$$

As regarding to the power balance, the relation of the supplied voltages for both windings is

$$V_a = aV_m \tag{2}$$

Therefore with the three-leg VSI and unbalanced SVPWM, the unbalanced two-phase outputs can be straightforwardly controlled to meet the relation in (2).

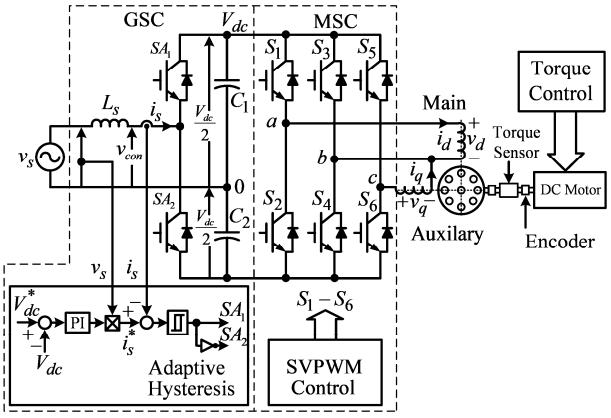

Fig.1. Proposed system

Adaptive hysteresis band current control [19]

In this paper, the DC link voltage is controlled to be constant using a PI controller together with adaptive hysteresis band current controller for the GSC. The principle of an adaptive hysteresis band current control technique can be explained as follows.

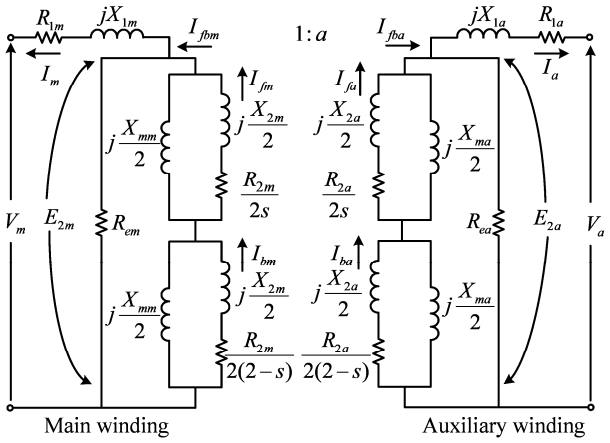

Fig.2. Steady state equivalent circuit for both windings of the unsymmetrical TPIG

An adaptive band hysteresis current control technique is modified from a fixed hysteresis band technique so as to improve performance such as current ripple due to irregular switching frequency. In order to achieve unity grid power factor, the equations for determining adaptive hysteresis band can be derived as follows. Firstly, let single-phase instantaneous grid voltage is

$$v_s = V_p \sin \omega t \tag{3}$$

Then the reference current for only real power transferred from the generator to the grid (i.e. without transferred reactive power) can be expressed as

(4) $$i_s^* = I_p \sin(\omega t - \pi)$$

Basic principle of fixed hysteresis band current control and corresponding converter voltage is shown in Fig.5.

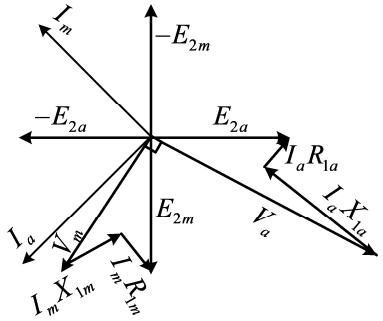

Fig.3. Corresponding phasor diagram for unsymmetrical TPIG with unbalanced supplied voltages under steady state conditions

In this scheme, the hysteresis bands are fixed throughout a fundamental period. In any switching period, the process of current control can be explained as follows. According to the GSC in Fig.1 when the switch SA_1 is turned on whilst the switch SA_2 is turned off, the converter voltage v_{con} changes from $-V_{dc}/2$ to $+V_{dc}/2$. As a consequence, the actual grid current rises linearly from point 1 in order to track the sinusoidal grid reference current. When the actual current hits the upper band at point 2, the switch SA_2 is turned on whilst the switch SA_1 is turned off. Subsequently the actual grid current falls linearly until it hits the lower band at point 3 in which the process completes one period of switching. Then the next process for the next period will be the same manner to track the reference sinusoidal current to be out of phase with respect to the grid voltage. The derivative of the actual grid current derived from the voltage across the inductor can be expressed as

(5) $$\frac{di_s}{dt} = \frac{1}{L_s}(v_{con} - v_s)$$

where

(6) $$v_{con} = \begin{Bmatrix} \frac{V_{dc}}{2} ON \\ -\frac{V_{dc}}{2} OFF \end{Bmatrix}$$

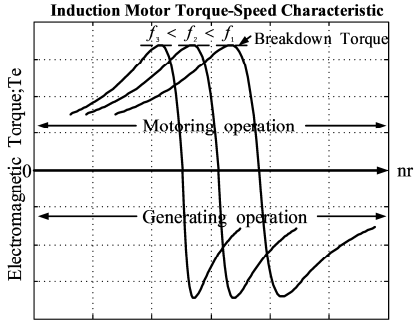

Fig.4. Torque-speed characteristics under variable speed operation of an induction machine

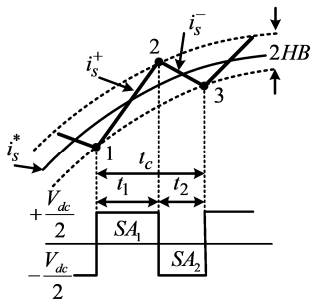

Fig.5. Fixed band hysteresis current control and converter voltage

From Fig.6, using the geometry yields

(7) $$\frac{di_s^+}{dt} = \frac{1}{L_s}(V_{dc} - v_s)$$

(8) $$\frac{di_s^-}{dt} = \frac{-1}{L_s}(V_{dc} + v_s)$$

(9) $$\frac{di_s^+}{dt} \times t_1 - \frac{di_s^*}{dt} \times t_1 = 2HB$$

(10) $$\frac{di_s^-}{dt} \times t_2 - \frac{di_s^*}{dt} \times t_2 = -2HB$$

The switching frequency is

(11) $$f = \frac{1}{t_1 + t_2}$$

By using (7)-(11), the hysteresis band can be achieved as

(12) $$HB = \frac{V_{dc}}{8fL_s} - \frac{L_s}{2fV_{dc}}\left(\frac{v_s}{L_s} + \frac{di_s^*}{dt}\right)^2$$

As shown in Fig.7 (a), the current error of fixed hysteresis band of $\pm 0.5A$, the switching frequency varies over a fundamental period which the minimum switching frequency is at $t=\pi/2,\ 3\pi/2$, etc. and the maximum switching is at $t=0,\ \pi,$ etc.

From Fig.7 (b), quite clearly at around the peak of positive and negative half cycle of the actual current, low switching frequency is present. Subsequently, it causes harmonics at low frequency resulting in an increase in total harmonic distortion. As shown in Fig.8 the instantaneous switching frequency of PWM pulses for several cycles of sinusoidal reference current is calaculated and plotted. Evidently, the variation of switching frequency is large. In order to remedy this problem, the adaptive band can be introduced.

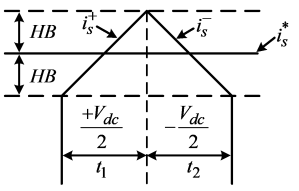

Fig.6. Upper and lower bands and corresponding time intervals for fixed hysteresis band

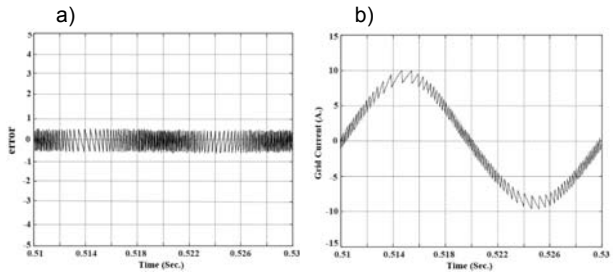

Fig.7. (a) Current error for fixed hysteresis band current control, (b) Actual current

From (4), the derivative of the reference current is expressed as

$$\frac{di_s^*}{dt} = \omega I_p \cos(\omega t - \pi) \tag{11}$$

Substituting (3) and (11) in (12), the complete expression of hysteresis band can be derived to be

$$HB = \frac{V_{dc}}{8fL_s} - \frac{L_s}{2fV_{dc}}\left(\frac{V_p \sin\omega t}{L_s} + (-\omega I_p)\cos\omega t\right)^2 \tag{12}$$

By using the relation of trigonometry in (13), hysteresis band from (12) can be formed as (14)

$$(A\sin\omega t + B\cos\omega t)^2 = \frac{1}{2}(A^2 + B^2)[1 - \cos 2(\omega t + \varphi)] \tag{13}$$

$$HB = (A - B) + B\cos 2(\omega t + \varphi)] \tag{14}$$

where

$$A = \frac{V_{dc}}{8fL_s} \tag{15}$$

$$B = \frac{L_s}{2fV_{dc}}\left(\left(\frac{V_p}{L_s}\right)^2 + (-\omega I_p)^2\right) \tag{16}$$

$$\varphi = \tan^{-1}\frac{-\omega I_p}{\left(\frac{V_p}{L_s}\right)} \tag{17}$$

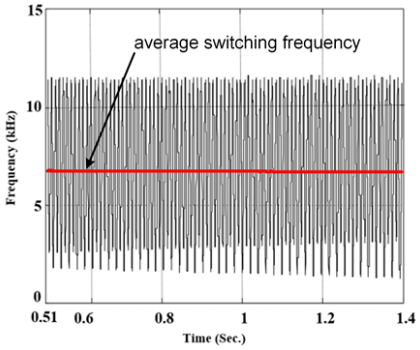

Fig.8. Instantaneous switching frequency and average switching frequency for fixed hysteresis band current control

According to (14), obviously, with a given switching frequency, modulation of HB occurs at twice the grid frequency with the average value A-B. For example, by setting the coefficients A and B with the same parameters as the fixed hysteresis band, the current error of adaptive hysteresis band can be plotted as shown in Fig.9. Obviously, HB varies with twice the grid frequency. The corresponding band shape is illustrated in Fig.10. Clearly at the peak of the positive and negative half cycle, the hysteresis band is minimum whist at $t=0$, π, etc., the hysteresis band is maximum. The corresponding actual current is illustrated in Fig.11. As can be seen, at the minimum hysteresis band, the switching frequency is increased. It implies that large harmonic distortion associated with fixed hysteresis band is remedied.

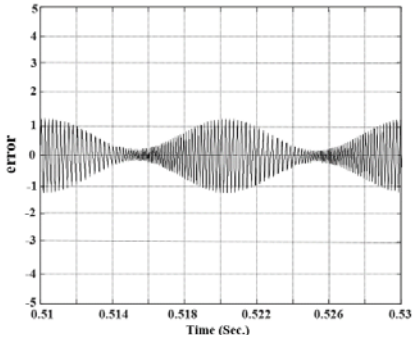

Fig.9. Current error of adaptive hysteresis band current control

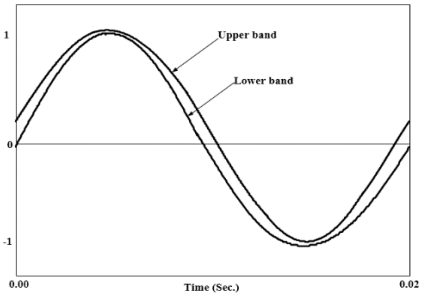

Fig.10. Band shape of adaptive hysteresis band current control

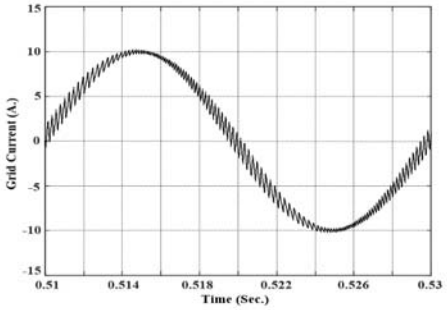

Fig.11. Actual current for adaptive band hysteresis current control

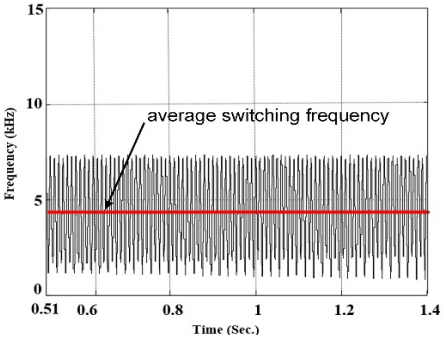

Fig.12. Instantaneous switching frequency and average switching frequency for adaptive hysteresis band current control

The corresponding instantaneous switching frequency of PWM pulses for several cycles of sinusoidal reference current is calculated and plotted as shown in Fig.12. When comparing the switching frequency characteristics between fixed and adaptive hysteresis bands, according to Figs.8 and 11, with the same reference current, the adaptive band hysteresis current control offers lower average switching frequency and lower variation of switching frequency (i.e. a range between maximum swithcing frequency and minimum switching frequency). This implies that this scheme gives lower switching loss.

Implementation of Time Based SVPWM for Two-Phase Three-leg VSI

A SVPWM technique for two-phase three-leg VSI is employed to provide balanced and unbalanced outputs [3, 6, 7, 24]. The voltage vectors and reference output voltage (V_o) in d-q plane for balanced and unbalanced outputs are illustrated in Figs.13 and 14, repectively. Voltage vectors consist of six active voltage vectors (SV_1-SV_6) and two zero voltage vectors (SV_0-SV_6) formed as asymmetric hexagon. For balanced voltages, the reference output voltage rotates with angular frequency (□) in a circular loci (i.e. orthogonal voltages and V_d=V_q) whilst for unbalanced voltages, the reference output voltage rotates in an elliptical shape (i.e. orthogonal voltages and V_q>V_d). The unbalanced SVPWM is modified from balanced SVPWM by shifting the axes of SV_3 and SV_6 with angle ϕ.

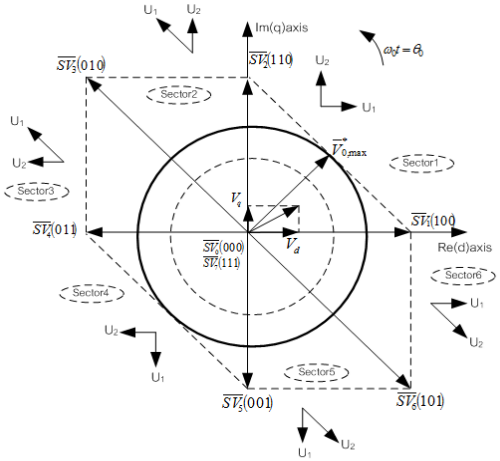

Fig.13. Location of voltage vectors in d-q plane for balanced SVPWM for two-phase three-leg VSI

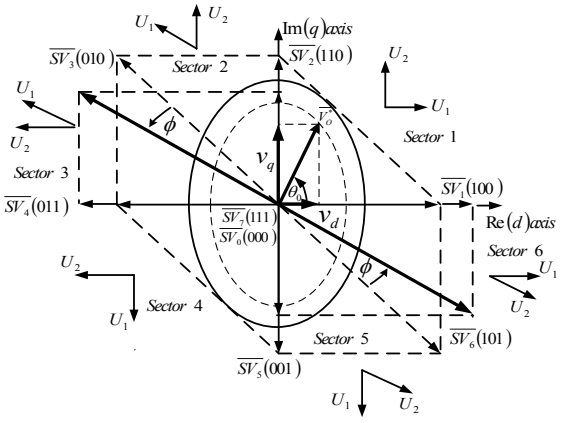

Fig.14. Location of voltage vectors in d-q plane for unbalanced SVPWM for two-phase three-leg VSI

Table 1. Voltage vectors $\bar{U}_1$ and $\bar{U}_2$ for switching time calculations

Sectors	$\bar{U}_1$	$\bar{U}_2$	T_1	T_2	V_1	V_2	α_1	α_2
1	$\overline{SV_1}(100)$	$\overline{SV_2}(110)$	T_{SV1}	T_{SV2}	$\frac{2V_{dc}}{\lvert A\rvert}$	$\frac{2V_{dc}}{\lvert B\rvert}$	0	$\frac{\pi}{2}$
2	$\overline{SV_3}(010)$	$\overline{SV_2}(110)$	T_{SV3}	T_{SV2}	$\frac{2V_{dc}}{\lvert C\rvert}$	$\frac{2V_{dc}}{\lvert B\rvert}$	$\frac{3\pi}{4}+\phi$	$\frac{\pi}{2}$
3	$\overline{SV_3}(010)$	$\overline{SV_4}(011)$	T_{SV3}	T_{SV4}	$\frac{2V_{dc}}{\lvert C\rvert}$	$\frac{2V_{dc}}{\lvert A\rvert}$	$\frac{3\pi}{4}+\phi$	π
4	$\overline{SV_5}(001)$	$\overline{SV_4}(011)$	T_{SV5}	T_{SV4}	$\frac{2V_{dc}}{\lvert B\rvert}$	$\frac{2V_{dc}}{\lvert A\rvert}$	$\frac{3\pi}{2}$	π
5	$\overline{SV_5}(001)$	$\overline{SV_6}(101)$	T_{SV5}	T_{SV6}	$\frac{2V_{dc}}{\lvert B\rvert}$	$\frac{2V_{dc}}{\lvert C\rvert}$	$\frac{3\pi}{2}$	$\frac{7\pi}{4}+\phi$
6	$\overline{SV_1}(100)$	$\overline{SV_6}(101)$	T_{SV1}	T_{SV6}	$\frac{2V_{dc}}{\lvert A\rvert}$	$\frac{2V_{dc}}{\lvert C\rvert}$	2π	$\frac{7\pi}{4}+\phi$

The desired output voltage in a vector form can be expressed with the sum of two-adjacent voltage vectors as

$$\bar{V}_o^* = V_o \angle \theta_o = \frac{T_1}{\Delta T/2}\bar{U}_1 + \frac{T_2}{\Delta T/2}\bar{U}_2 \tag{18}$$

Two adjacent voltage vectors in an exponential form are expressed as

$$\bar{U}_1 = V_1 e^{j\alpha_1} \tag{19}$$

$$\bar{U}_2 = V_2 e^{j\alpha_2} \tag{20}$$

Switching time intervals can be expressed as

$$\Delta T/2 = T_1 + T_2 + T_0 + T_7 \tag{21}$$

The amplitude of the output voltage can be determined from

$$V_o = \sqrt{V_d^2 + V_q^2} \tag{22}$$

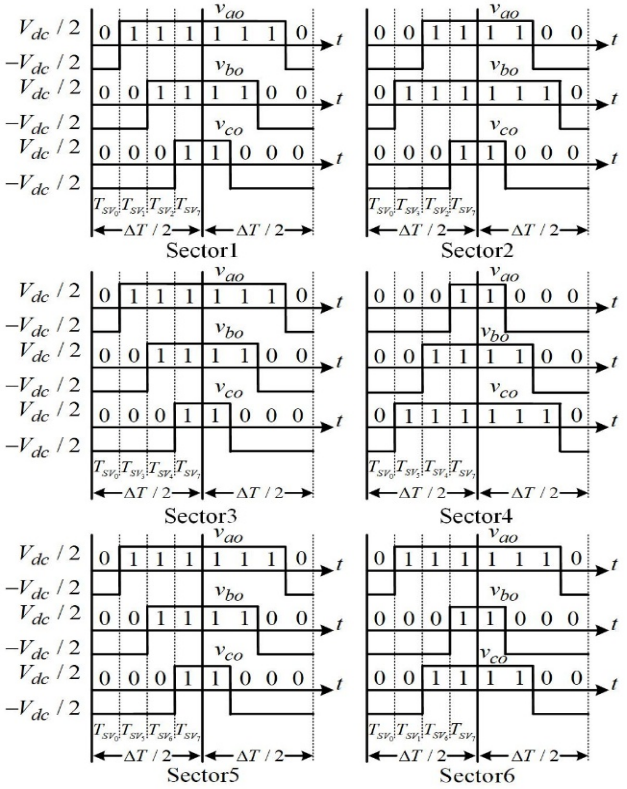

Fig.15. Example of Phase leg voltages in a period of sampling for each sector

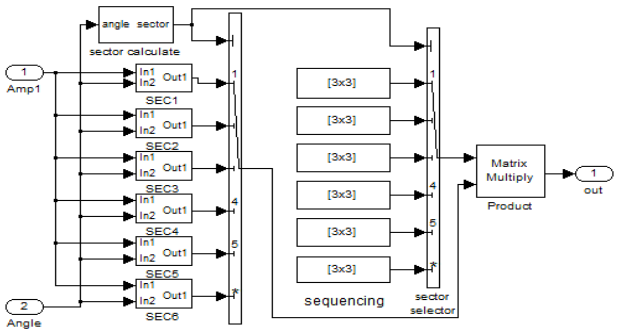

Fig.16 Time based PWM generator using space vector PWM.

By using Table1 together with (18) -(21), switching times for voltage vectors can be determined. Fig.15 illustrates example of phase leg voltages of the inverter. By using voltage vectors and corresponding switching times, SVPWM patterns are generated by TMS320C2000 F28335 microcontroller boards. The program is written using SIMULINK as shown in Fig.16 [5].

Simulation and Experimental Results

The performance analysis of the proposed system has been verified by both simulation and experiment. The simulation has been conducted through MATLAB/Simulink. The experimental setup of the proposed system is shown in Fig.17. The system mainly consists of two sets of IGBT converters for front side and machine side, two capacitors connected in series for DC link filter elements to form a double voltage configuration, a two-phase induction generator modified from an existing SPIM, a DC motor, an inductor for grid interface and various instruments. The DC motor driven by SIMOREG DC Master6RA70 Series Siemens dual thyristor converter acts as a prime mover. The shaft torque and speed are measured by a torque transducer and a tachometer, respectively for measuring the mechanical input power. Four channel digital oscilloscopes are used to record voltage and current waveforms.

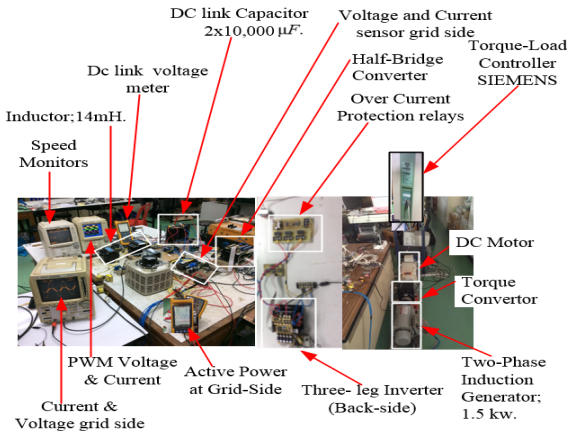

Fig.17. Photograph of experimental setup

The electrical output power is measured by using a power analyzer. With this power quality instrument, harmonic spectrum of currents is also analyzed. The switching frequency of SVPWM for the MSC is fixed at 5 kHz which is reasonable for switching and harmonic loss considerations. The DC link voltage is kept constant at 700 V in order to obtain a full flux level of excitation under various frequency conditions of the induction generator. The parameters of the induction generator and the front end converter are shown in Table2 and Table3, respectively. Winding voltage and current waveforms of the induction generator at 30 Hz and rated input torque of 9 Nm are shown in Figs.19 and 20 for balanced and unbalanced SVPWM, respectively. The simulation and experimental results are almost identical. The winding current waveforms for unbalanced SVPWM are less distorted than those for balanced SVPWM. Winding voltage and current waveforms of the induction generator are shown in Figs. 20 and 21 for balanced and unbalanced SVPWM, respectively. Again, the simulation and experimental results are almost identical. The winding current waveforms for unbalanced SVPWM are still less distorted than those for balanced SVPWM for rated frequency of excitation. According to these results of both simulation and experiment confirm the correctness of implementation and validity of obtained parameters for a model. Unbalanced SVPWM shows better performance in terms of motor currents. This implies that unbalanced SVPWM could reduce electromagnetic torque ripple.

Table 2. The parameters of the induction generator

Parameter	Value
Induction motor 1 phase	1.5 kW
Rated voltage	220 V_{rms}
Rated current	9.8 A
Maximum torque	9.5 Nm
Poles	4
Rated speed, n_r	1450 rpm
Main winding resistance, R_{sd}	1.59 Ω
Main winding inductance, L_{sd}	5.96 mH
Auxiliary winding resistance, R_{sq}	5.10 Ω
Auxiliary winding inductance, L_{sq}	15.91 mH
Moment inertia, J	0.025kgm^2
Turn ratio, a	1.556

Table 3. Parameters of the half-bridge front-end converter

Parameter	Value
Grid voltage, v_s	220 V_{rms}
Frequency	50 Hz
Rated inductance, L_s	14 mH
Rated Current, i_s	10 A
Rated capacitor C_1 and C_2	10,000μF
DC link voltage, V_{dc}	700V

The capacitor voltages, DC link voltage and converter voltage for balanced SVPWM and unbalanced SVPWM are illustrated in Figs. 22 and 23, respectively. The simulation and experimental results are in good agreement. Clearly, unbalanced SVPWM gives remarkably lower voltage ripple. Note that DC link voltage affects the quality of motor voltage and grid current. Two level PWM voltage of the GSC associated with hysteresis current control can be obviously seen in accordance with Fig.5. Figs. 24 and 25 show simulation and experimental results of grid voltage and current waveforms and corresponding harmonic current contents for fixed hysteresis band current control respectively. The simulation and experimental results are in good agreement. Figs. 26 and 27 show results of simulation and experiment of grid voltage and current waveforms and corresponding harmonic current contents for adaptive hysteresis band current control, respectively. Again, the simulation and experimental results are in good agreement. Clearly, according to harmonic spectrum of the grid current, adaptive hysteresis band current control gives lower total harmonic distortion. These results confirm the capability of adaptive hysteresis band of a reduction in harmonics of the grid current.

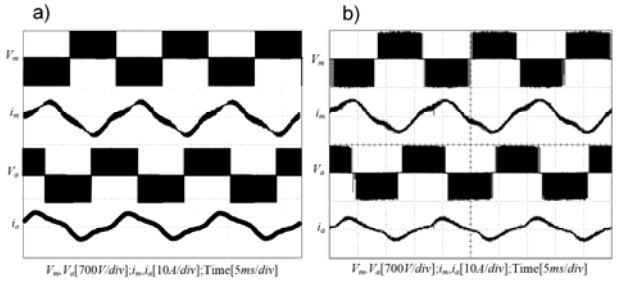

Fig.18. (a) Simulation results of winding voltages and currents for balanced SVPWM at generator frequency of 30 Hz, (b) Measured results of winding voltages and currents for balanced SVPWM at generator frequency of 30 Hz

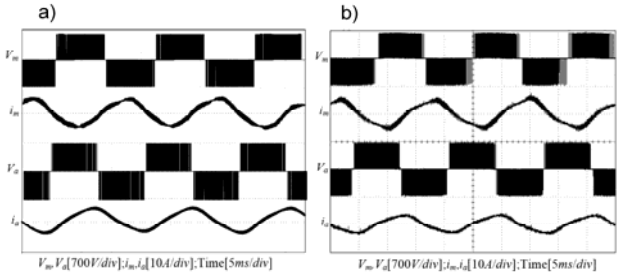

Fig.19. (a) Simulation results of winding voltages and currents for unbalanced SVPWM at inverter frequency of 30 Hz, (b) Measured results of winding voltages and currents for unbalanced SVPWM at inverter frequency of 30 Hz

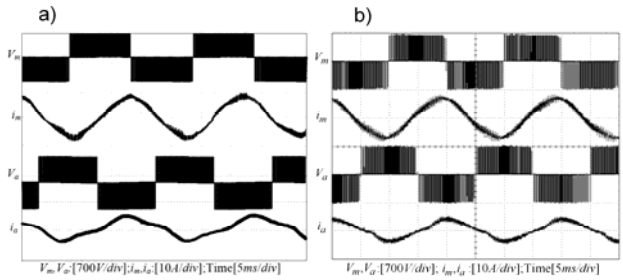

Fig.20. (a) Simulation results of winding voltages and currents for balanced SVPWM at inverter frequency of 50 Hz, (b) Measured results of winding voltages and currents for balanced SVPWM at inverter frequency of 50 Hz

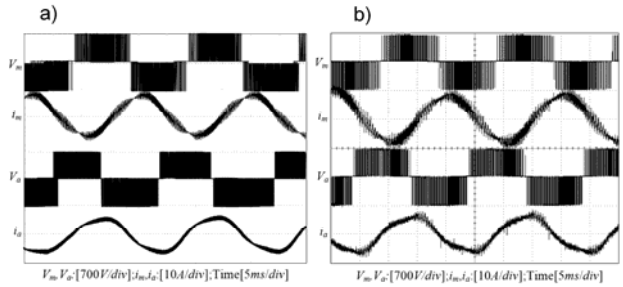

Fig.21. (a) Simulation results of winding voltages and currents for unbalanced SVPWM at generator frequency of 50 Hz, (b) Measured results of winding voltages and currents for unbalanced SVPWM at generator frequency of 50 Hz

Grid power and power factor can be seen in Fig.28 (a) and (b) for balanced SVPWM and unbalanced SVPWM at the generator frequency of 50 Hz and the mechanical input torque of 9 Nm. Obviously, at the same torque value, unbalanced SVPM gives higher transferred power form the generator to the grid. It means that the proposed unbalanced SVPWM gives higher efficiency. Fig.29 shows a comparison of performance between balanced SVPWM and unbalanced SVPWM with variation of rotor speed at various generator frequencies. The characteristics are in accordance with Fig.4 for the regeneration mode. Again at the same frequency and the same rotor speed, unbalanced SVPWM requires lower mechanical input torque resulting in lower power input. It implies that higher efficiency of the proposed system can be achieved due to lower input power and higher transferred grid power. According to these results the unbalanced space vector PWM outperforms balanced one.

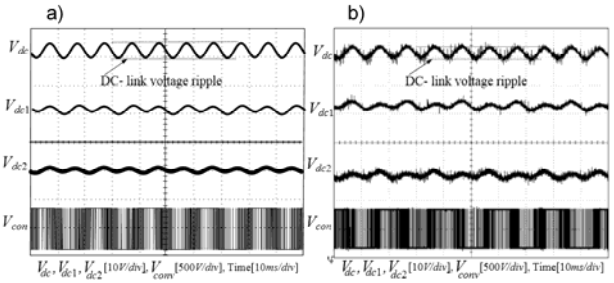

Fig.22. (a)Simulation results of dc link voltage and converter voltage for balanced SVPWM, (b) Measured results of dc link voltage and converter voltage for balanced SVPWM

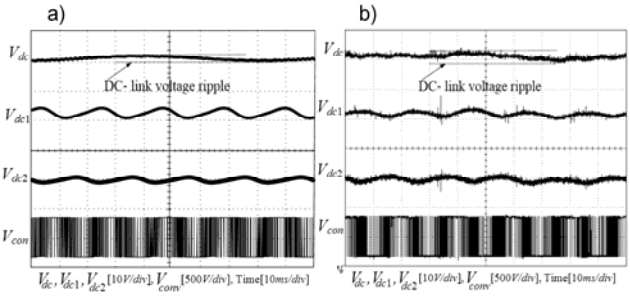

Fig.23 (a)Simulation results of dc link voltage and converter voltage for unbalanced SVPWM, (b) Measured results of dc link voltage and converter voltage for adaptive band hysteresis current control

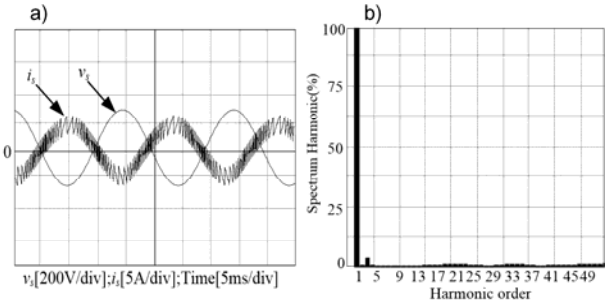

Fig.24. (a) simulation results of grid voltage and current waveforms for fixed band hysteresis current control, (b) Corresponding harmonic spectrum of grid current with THDi of 16.5 %

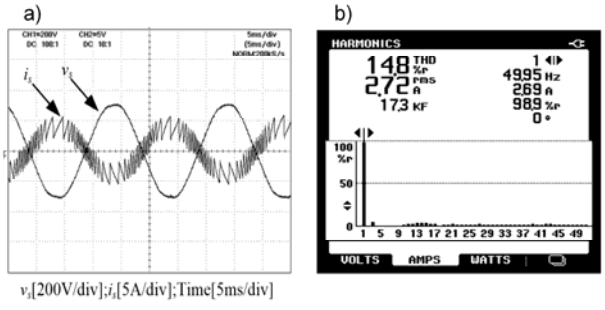

Fig.25. (a) Measured grid voltage and current waveforms for fixed band hysteresis current control, (b) Corresponding harmonic spectrum of grid current

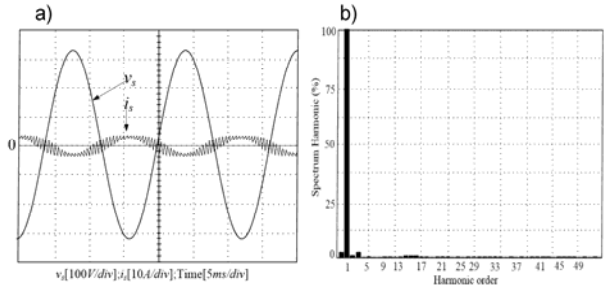

Fig.26. (a) Simulation results of grid voltage and current waveforms for adaptive band hysteresis current control, (b) Corresponding harmonic spectrum with THDi of 13.1%

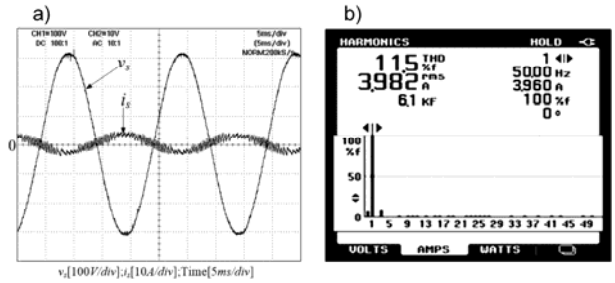

Fig.27. (a) grid voltage and current waveforms for sinusoidal hysteresis band current control, (b) Corresponding harmonic spectrum of grid current

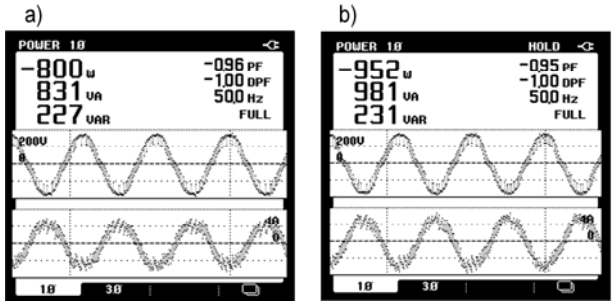

Fig.28. (a) Grid power and Power factor for balanced SVPWM, (b) Grid power and Power factor for unbalanced SVPWM

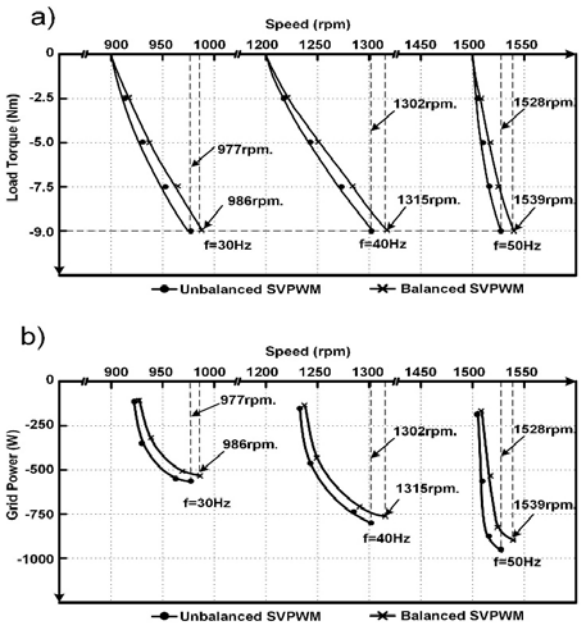

Fig.39. (a) Comparison of torque-speed characteristics between B-SVPWM and UB-SVPWM, (b) Comparison of grid power-speed characteristics between B-SVPWM and UB-SVPWM

Conclusion

This paper has presented performance analysis of a single-phase grid connected unsymmetrical two-phase induction generator using a DC-AC-AC system. An adaptive band hysteresis current control technique is used for a voltage doubler rectifier with regenerative operation for power transfer from the induction generator to the grid. The adptive band hysteresis current controller offers lower total harmonic distortion of the grid current and lower average switching frequency thus lower switching loss. For variable frequency excitation of the generator, time-based SVPWM is generated by a low cost microcontroller applied to a three-leg VSI providing unbalanced two-phase voltages resulting in better performance in terms of voltage and current waveforms of the generator, DC link voltage ripple, transferred grid power when compared to balanced two-phase voltages.

Nomenclature

v_s, v_{con}	Instantaneous grid and converter voltage
V_{dc}^* , V_{dc}	DC reference and DC link voltage
i_s	Instantaneous grid current
v_d, v_q	Instantaneous direct and quadrature axes stator voltages
i_d, i_q	Peak currents of main and auxiliary windings
L_S	Coupling inductance
t_1 , t_2	Switching time intervals
f	Switching frequency
i_s^*, i_s^+, i_s^-	Reference sinusoidal, rising and falling currents, respectively
ω	The angular frequency of grid
a	Turns ratio of auxiliary to main windings
s	Rotor slip
J	Moment inertia
V_m, V_a	Voltages of auxiliary and main windings, respectively
I_m, I_a	Main and auxiliary winding currents
R_{1m}, R_{1a}	Resistances of the main and auxiliary windings, respectively
X_{1m}, X_{1a}	Leakage reactance of the main and auxiliary windings, respectively
X_{2m}, X_{2a}	Rotor leakage reactance referred to stator
X_{mm}, X_{ma}	Magnetizing inductance
R_{2m}, R_{2a}	Rotor resistance referred to stator
E_{2m}, E_{2a}	Induced electromotive force (EMF)
I_{fm}, I_{fa}	Forward current
I_{bm}, I_{ba}	Backward current
V_1,V_2	Magnitude of two adjacent active voltage vectors
α_1,α_2	Angles of two adjacent active voltage vectors
$\bar{U}_1$,$\bar{U}_2$,	Two adjacent voltage vectors
T_1,T_2	Switching time
$\overline{SV_1} - \overline{SV_6}$	Six active voltage vectors

Acknowledgement

The authors wish to thank school of engineering, King Mongkut's Institute of Technology Ladkrabang for financial support.

Authors: *Mr. Narongchai Thodsaporn, Department of Electrical Engineering, School of Engineering, King Mongkut's Institute of Technology Ladkrabang, E-mail: knarongchai@gmail.com; Prof.Dr.Vijit Kinnares, Department of Electrical Engineering, School of Engineering, King Mongkut's Institute of Technology Ladkrabang, E-mail: kkwijit@kmitl.ac.th; Asst.Prof.Dr.Papol Sardyoung, Faculty of Industrial Technology, Thepsatri Rajabhat University, E-mail: papol_s@hotmail.com;*

REFERENCES

[1] Sen, P.C. Principle of electric machines and power electronics, John Wiley & Sons 3rd edition 2013

[2] Sardyoung, P., Kinnares, V., Control of a converter system for an asymmetrical parameter type two-phase induction motor drive operating in motoring and generating modes, *Journal of the Chinese Institute of Engineers*, (2018), Vol.41, 86-97

[3] Khongsuk**,** P., Kinnares, V., Phumipkak, P., Performance Evvaluation of Three-PhaseVoltage Voltage Source Inverter fed Unsymmetrial Two-Phase Induction motor Based on Genetic Algorithm for Parameter Estimation, *Advanced in Electrical and Electronic Engineering*,Vol.17, No.4, December, 2019

[4] Muangthong, K., Charumit, C., Comparative analysis of switching losses and current ripple of continuous and discontinuous SVPWM strategies for unbalanced two-phase four-leg VSI Fed unsymmetrical two-phase induction motor, *IET Power Electronics*, 14 (2020), 531-547

[5] Chiyot, R., Kinnares, V., Continuous and Discontinuous Space Vector Pulse Width Modulator using a TMS320C2000 F28335 Board, *13th International Conference on Electrical Engineering/Electronics, Computer, Telecommunications and Information Technology (ECTI-CON),* 2016

[6] Kumsuwan, Y., Premrudeepreechacharn, S., Kinnares, V., A Carrier-Based Unbalanced PWM Methofor Four-Leg Voltage Source Inverter Fed Unsymmetrical Two-Phase Induction Motor, *IEEE Trans. Ind. Electron*., 60 (2013), No. 5, 2031-2041

[7] Naser, M.B., Rahim, A., An Unsymmetrical Two-Phase Induction Motor Drive With Slip-Frequency Control, *IEEE Transaction on Energy Conversion*, Vol.24, No.3, Sep., 2009

[8] Balamurugan, K., Slochanal, S.M.R., Amutha, N., Design of Grid-Connected Induction Generators for Variable Speed Wind Power Generation, *International Energy Journal*, 9 (2008), 59-64

[9] Almarshoud, A.F., Abdel, H.M.A., Alolah, A.I., Performance of Grid-Connected Induction Generator under Naturally Commutated AC Voltage Controller, *Electric Power Components and Systems*, 32 (2004), 691-700

[10] Gorski, D.A., Balkowiec, T., Koczara, W., Grid Connection of a Converter Controlled Squirrel-Cage Induction Generator, *7th International Conference on Renewable Energy Research and Applications (ICRERA)*, (2018), 348-353

[11] Singh, A., Ahuja, H., Bhadoria, V., Singh, S., Control Implementation of Squirrel Cage Induction Generator based Wind Energy Conversion System, *Journal of Scientific and Industrial Research*, 79(2020), 306-311

[12] Sikrski,S., Kuźma, A., Cooperation of induction squirrel-cage generator with grid connected AC / DC / AC converter, *Bull. Pol. Ac.: Tech.*, 57 (2009), No.4, 317-322

[13] Yukhalang, S., Sawetsaklanond B., Kinnares, V., Performance Evaluation of a Single-Phase Grid Connected Induction Generator, *17th International Conference on Electrical Machines and Systems (ICEMS)*, (2014), 3148-3153

[14] Madawal, U.K., Bradshaw, J.B., Vilathgamuwa, D.M., Modeling and Analysis of a Novel Variable-Speed Cage Induction Generator, *IEEE Trans. On Industry Applications*, 59 (2012), No.2, 1020-1028

[15] Nuttapong, P., Sawetsakulanond, B., Kinnares, V., Analysis and investigation on the behavior and performance of single phase grid connected induction generators system, *20th International Conference on Electrical Machines and Systems (ICEMS),* (2017)

[16] Prapurt, N., Sawetsakulanond, B., Kinnares, V., Power Factor Improvement and Inrush Current Reduction of a Grid Connected Split-Phase Induction Generator, *21st International Conference on Electrical Machines and Systems (ICEMS)*, (2018), 1060-1064

[17] Shiddiq, Y.A.F., Swasti, S., Purwito, Overview of Hysteresis Current Controller Application in Renewable Energy Based Power Systems, *I-COSINE*, 536(2019),1-8

[18] Mohaptra, M., Babu, B.C., Fixed and Sinusoidal-Band Hysteresis Current Controller for PWM Voltage Source Inverter With LC Filter, *IEEE Students Technology Symposium*,(2010)

[19] Bose, B.K., An Adaptive Hysteresis-Band Current Control Technique of a Voltage-Fed PWM Inverter for Machine Drive System, *IEEE Transaction on Industrial Electronics*, 37 (1990), No.5, 402-408

[20] Jabbar, A.F., Mansor, M., Current control loop of 3-Phase grid-connected inverter, *4th International Conference on Energy and Environment,* (2013), 1-4

[21] Hassan, S., Implementation of Adaptive Hysteresis Current Controlled Shunt Active Filter for Non-Linear Loads, *International Journal of Innovative Research in Electrical, Electronics, Instrumentation and Control Engineering*, 2 (2014), No. 2, 1089-1093

[22] Wannakarn, P., Kinnares, V., Single-Phase Grid Connected Axial Flux Permanent Magnet Generator System with Harmonic Mitigation Functionality for Various Types of Nonlinear Loads, *International Review of Electrical Engineering* (IREE), 13 (2018), No.2, 157-164

[23] Dangeam, S., Kinnares, V., Implementation of a drive system for dual single-phase induction motor using a five-leg inverter with carrier-based space vector PWM technique, *Przeglad Elektrotechniczny,* 2021 (2021), No. 1, 78-85

[24] Charumit, Ch., Kinnares, V., Carrier-based unbalanced phase voltage space vector PWM strategy for asymmetrical parameter type two-phase induction motor drives, *Science Direct, Electric Power Systems Research*, 79 (2009), No. 7, 1127-1135